The experimental dielectric function of porous anodic alumina in the infrared region; a comparison with the Maxwell-Garnett model

1996 J. Phys.: Condens. Matter 8 4289

(http://iopscience.iop.org/0953-8984/8/23/019)

J. Phys.: Condens. Matter **8** (1996) 4289–4299. Printed in the UK

The experimental dielectric function of porous anodic alumina in the infrared region; a comparison with the Maxwell-Garnett model

Ewa Wäckelgård

Solid State Physics, Department of Technology, Box 534, Uppsala University, S-751 21, Uppsala, Sweden

Received 23 November 1995, in final form 14 March 1996

Abstract. The infrared reflectance from thin alumina films on metal substrates has a deep minimum for p-polarized light at oblique incidence. This originates from absorption when light couples with a longitudinal optical (LO) phonon mode with $\boldsymbol{k}$-vector zero. The absorption band is wide for amorphous alumina and is shifted to longer wavelengths for porous oxides compared to non-porous ones. Anodic alumina, prepared in phosphoric acid, with a pore volume fraction of 0.3, has been investigated. The s- and p-polarized reflectance has been measured for selected angles of incidence between 15° and 75°, and the dielectric function has been determined from these measurements. The effective dielectric function has been calculated using Maxwell-Garnett effective-medium theory for a two-component anisotropic medium consisting of air-filled cylindrical pores perpendicular to the surface in an alumina matrix with optical constants of non-porous evaporated alumina. The theoretical and experimental results are in good agreement, which shows that the redshift of the LO mode absorption for p-polarized light can be explained by the presence of pores.

1. Introduction

Alumina is used in a variety of technical applications, which has made it the focus of rigorous investigations covering many aspects, including its optical characteristics. The most complete set of optical infrared measurements has been performed on single-crystal α-alumina [1]. From dispersion analyses using the Lorentz oscillator model, the frequencies were found for the transverse optical phonon modes (the TO modes) at wavevector zero with the electric field perpendicular or normal to the c-axis of the crystal. In total six modes exist. The longitudinal optical phonon (LO mode) frequencies were taken from the zeros of the real part of the dielectric function. Other crystalline phases of alumina, such as γ-alumina for which four optically active modes have been determined, have also been investigated by dispersion analysis [2].

In the case of crystalline bulk dielectrics, the interaction between the electromagnetic field and the optical phonon modes is manifested by a high reflectance in the frequency range between the transverse and longitudinal optical phonon modes. This is called the reststrahlen band. The high reflectance originates from the inability of waves to propagate in the forbidden bandgap between the TO and LO frequencies. The infrared optical properties of amorphous alumina, prepared by thermal oxidation, anodization, evaporation or sputtering, have also been studied. Amorphous alumina which is thick enough to be considered to have bulk optical properties in the infrared, has a much lower reflectance in the reststrahlen band

0953-8984/96/234289+11$19.50

than crystalline alumina [3]. This can be explained by the large energy dissipation caused by phonon scattering in a system with only short-range order.

However, if the film is thinner, less then 1 μm, which is common in many of the reports on amorphous alumina, a reststrahlen band is not observed since waves can actually propagate through matter with a thickness much smaller than the wavelength of the wave [4]. Instead, the transmittance in this wavelength range is high, except at the wavelengths around the TO and LO modes respectively, where light is absorbed [4] because of phonon scattering processes. LO modes can only be excited for p-polarized light, at non-normal angles of incidence, which has been used to determine the frequencies of the LO modes directly from transmittance or reflectance spectral measurements on thin alumina films [5–9]. The LO absorption has a large bandwidth for amorphous alumina so it is impossible to resolve more than the highest-frequency LO mode which causes the strongest absorption. The location of TO modes has also been determined from s-polarized transmittance or reflectance measurements on samples with thicknesses that are small compared to the wavelength, but not thinner than about 0.5 μm [6, 5, 8]. It should be mentioned that the reflectance measurements must be made on samples on a metallic substrate, otherwise the thin-film approximation referred to [4] is not valid. Dispersion analysis has also been used for thin amorphous alumina films [10, 2] whereby optical constants have been determined using the Fresnel formalism for both evaporated [11] and anodized [12, 13] amorphous alumina.

From the reports referred to above, one can conclude that amorphous alumina has two optically active infrared modes. The stronger one is reported at about 650 cm^{-1} (15.4 μm), except on those occasions when dispersion analysis has been used. In these two cases it has been reported at 720 cm^{-1} (13.9 μm) [2] and 850 cm^{-1} (11.8 μm) [10]. In contrast, the frequency of the stronger LO mode is in surprisingly good agreement, regardless of the measuring technique or the data processing. In this case the different values seem to be related to the type of amorphous alumina. Evaporated, sputtered, thermal and barrier anodic oxides each have the maximum in the LO mode absorption reported at around 950 cm^{-1} (10.5 μm) [6, 9, 5, 8], but in anodic alumina formed in sulphuric acid, the maximum has shifted to a lower frequency, 920 cm^{-1} (10.9 μm), whilst when phosphor anodized, it has shifted to 880 cm^{-1} (11.4 μm) [7]. There is a significant morphological difference which could explain a shift of the LO mode: anodic alumina formed in sulphuric and phosphoric acid has pores perpendicular to the surface, with phosphoric acid having a larger pore fraction compared to alumina prepared in other acids [14, 15]. The diameter of the pores can be as large as 200 nm and constitute up to 40% of the total volume [16]. Therefore it can be hypothesized that the pores play a crucial role in the redshift of the LO mode. Another suggestion is that the LO mode is shifted because of differences between the chemical bonds of the non-porous and porous alumina. In the work presented here, theoretical modelling based on effective-medium theory has been used to explain the redshift of the LO mode frequency for porous alumina. The optical constants for evaporated alumina have been taken for these calculations to obtain the effective optical constants for porous oxide using the Maxwell-Garnett effective-medium model. The results are then compared with the experimentally determined optical constants for phosphor-anodized alumina.

2. Sample preparation and sample characterization

Rolled aluminium sheet plated with a 3 μm thick aluminium layer has been used as the substrate. The samples were anodized in 2.5 M phosphoric acid at a constant dc voltage of 15 V for 15 minutes at a temperature of 19.0 ± 0.5 °C. The current density was typically about 3.5 mA cm^{-2}. The oxide film thickness and surface roughness were then measured

with an Alpha-Step 200 stylus mechanical profilometer.

A distinct step from the oxide surface to the aluminium substrate was produced by selectively dissolving the oxide on part of the sample area in chromic phosphoric acid [15]. The oxide film thickness was found to be 0.50 ± 0.02 μm. The average surface roughness was 0.02 μm, both for the substrate and for the oxide surface.

The porous structure was investigated with scanning electron microscopy, SEM. Cracks in the oxide, made by bending the sample, revealed the cross-sectional structure. In common with previously published micrographs [17], [14], the micrographs showed channels of a fibrous nature in the oxide perpendicular to the surface.

The pore size was determined from transmission electron microscopy, TEM, pictures. Some aluminium oxide was stripped from the aluminium metal by amalgamation [15]. These oxide fragments were then rinsed in distilled water, placed on a copper wire grid and mounted in a TEM instrument. The pores in the oxide are electron transparent since there is only a thin barrier layer below the pore. The pores are not straight uniform cylinders perpendicular to the surface, which makes the estimation of pore size from these micrographs somewhat uncertain. Nevertheless, by measuring the number of bright spots on the micrographs and their width, the volume fraction of pores was found to be about 30% with an average diameter of 30 nm.

From grazing-incidence x-ray diffraction measurements it is clear that the aluminium oxide is amorphous. Some low-intensity peaks reveal some crystallization, although the peaks could not be identified as belonging to any one of the known phases of aluminium oxide or crystalline aluminium hydroxides or oxyhydroxides. It is known that the poorly crystalline pseudo-boehmite is formed during anodization [18], but after heating to 400 °C it is transformed into aluminium oxide. Since the diffraction peaks disappeared after the sample was heated to 400 °C, these peaks could belong to low concentrations of pseudo-boehmite.

3. Optical measurements

Specular reflectance was measured in the wavelength range 2–50 μm with a double-beam Perkin–Elmer 983 Infrared Spectrophotometer. The s- and p-polarized reflectance was measured in steps of 5° using a variable-angle-of-incidence accessory for angles between 15° and 75°. The measurements were repeated for each angle with a reference sample of evaporated aluminium on glass replacing the actual samples. The reflectance data for the samples were divided by the reference spectrum and multiplied by the calculated reflectance of aluminium using optical constants from the literature [19].

A scan mode was chosen with a resolution of 7 cm^{-1} at 1150 cm^{-1}. The stray light, as specified in the instrument manual, was less than 1% between 400 and 180 cm^{-1}, and was lower in the rest of the range measured. An upper limit of 0.01 was set for the absolute error in the reflectance throughout this range, regardless of the value of the reflectance. The angle setting for the variable-angle accessory could not be more accurate than within 0.5°.

The samples are highly specular; the diffuse reflectance was measured at 2.5 μm in a Beckman UV 5240 photospectrometer equipped with an integrating sphere. The diffuse component was 0.03 and the total reflectance 0.92. Therefore the reflectance can only be considered to be specular for longer wavelengths, as in the infrared wavelength range.

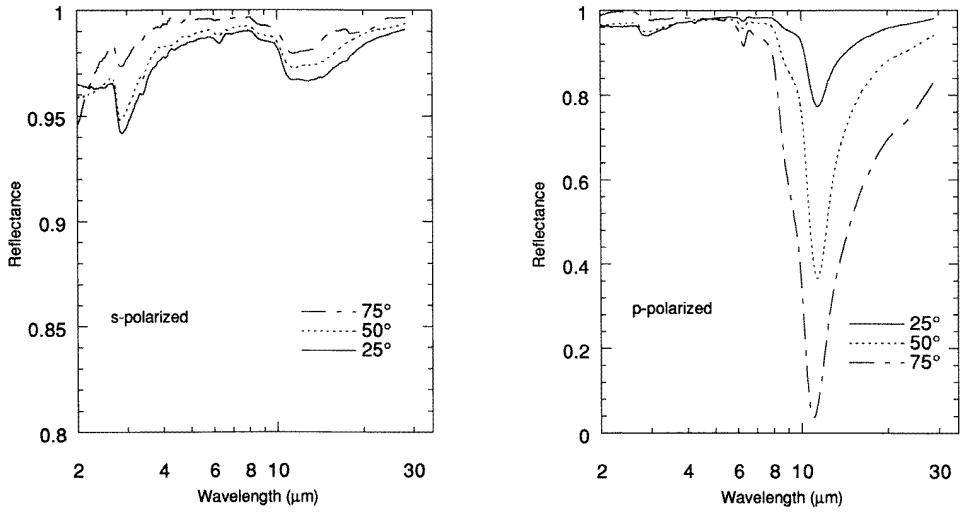

Figure 1. Specular reflectance of porous alumina for three different angles of incidence, in the s- and p-polarized cases.

4. Experimental results from optical measurements

The reflectance measurements are presented in figure 1 for s- and p-polarized light at angles of incidence of 25°, 50° and 75°. There is a broad reflectance minimum at 11.4 mm (880 cm^{-1}), which is strongly angle dependent, and, since it appears only for p-polarized light, it is identified as absorption by longitudinal optical phonons in the aluminium oxide. The wavelength of the peak absorption is the same as has been observed before for phosphor-anodized alumina [7]. A weak absorption band corresponding to the wavelength range of the TO mode appears as a shoulder on the long-wavelength side of the LO absorption. Both the LO and TO absorption bands of amorphous structures are much broader than for crystalline structures. Anions from the electrolytes PO_4^{3-}, HPO_4^{2-} and H_2PO^{4-} absorb in the region 9–10 μm (1100–1000 cm^{-1}) and are responsible for the absorption on the short-wavelength side of the reflectance minimum of the LO mode [20].

The pseudo-boehmite can be identified from absorption bands in the infrared wavelength range: the AlO–H stretching mode introduces a broad band centred at 3600 cm^{-1} (2.8 μm), the H–O–H bending, one at 1600 cm^{-1} (6.2 μm), and Al–OH bending forms a narrow band at 1040 cm^{-1} (9.6 μm). The latter cannot be resolved from the LO mode absorption band of the oxide [18].

From these infrared optical measurements it is evident that the main constituent of the material is amorphous aluminium oxide.

5. Determining the optical constants for porous alumina

Optical constants have been determined before for alumina films in the infrared wavelength region [11–13]. The method used for electron-beam-evaporated alumina [11] was to measure normal transmittance with oxide evaporated onto an infrared transparent substrate, and near-normal reflectance with a highly reflecting substrate. Anodic aluminium oxide can be detached from the aluminium substrate for transmittance measurements [12].

The phosphor-anodized alumina is anisotropic because the pore structure has pores preferentially oriented perpendicular to the surface. A uniaxial symmetry perpendicular to the surface can be described by two sets of complex refractive indices, one set parallel and the other perpendicular to the surface.

Optical constants can be derived solely from reflectance measurements. In this case, when four measurements are needed, one can use a combination of s- and p-polarized reflectance for two angles of incidence, or just p- or s-polarized reflectance for four different angles of incidence. The advantage of the reflectance method is that the alumina films do not need to be detached from the aluminium substrate. The disadvantage is that it can only be used for wavelengths with a significant difference in reflectance between the angles of incidence used [21]. This rules out s-polarized reflectance altogether since the angular dependence of the reflectance is very weak, as demonstrated in figure 1. In contrast, the p-polarized reflectance is strongly angle dependent in the region of the broad LO absorption band. Thus the combination of four p-polarized reflectance measurements was tried to obtain a fit to the data for the calculated reflectance of an anisotropic thin film on an aluminium substrate [22]. The film thickness was fixed to the value determined from the stylus profilometer measurement and the optical constants for the aluminium substrate were taken from the literature [19]. A Newton–Raphson iterative numerical method was used and the fitting was limited to the wavelength range 5–30 μm. However, the calculations did not converge, or converged to unphysical values, which showed that four variables was too many.

The number of variables was then reduced by taking the Fresnel equations for an isotropic film on an absorbing substrate into account. On using p-polarized light at high angles of incidence, the isotropic constants obtained for the film should be relatively close to the component perpendicular to the surface of the proper anisotropic set of optical constants.

The combination $R_p(75^\circ)/R_p(50^\circ)$ was used rather than one with angles even closer together, such as $R_p(75^\circ)/R_p(70^\circ)$, as this gave greater uncertainty in the refractive index since the reflectance for these two angles does not differ substantially.

To examine the validity of the optical constants determined with the chosen combination, the reflectance was also calculated for the remainder of the measured angles of incidence using the Fresnel formulae for isotropic films on aluminium. The result is shown in figure 2 for three selected angles. The calculated p-polarized reflectance is in good agreement with that measured, except for at the lowest angles. The reflectance for s-polarized light is high for all angles of incidence and it is seen that the calculated reflectance is systematically about 1–2% higher for the measured reflectance. There is also a small LO absorption in the experimental data which should not be present for pure s-polarized light.

6. Theory

The dielectric function calculated from the experimental complex refractive index is presented in figure 3. Error bars are drawn for some experimental points to show the level of uncertainty in different intervals. These were obtained for each point from the combination of $R^{exp} \pm 0.01, \theta \pm 0.5^\circ$ and the thickness ± 0.02 μm which gave the largest deviation in the refractive index. Error bars for shorter wavelengths are smaller than the size of the experimental points in the plot.

As mentioned above, experimental data do exist [11] for the dielectric function of amorphous evaporated alumina; these are also plotted in figure 3 for comparison. The dielectric functions of the non-porous and porous alumina have the same curvature, but differ in three important respects.

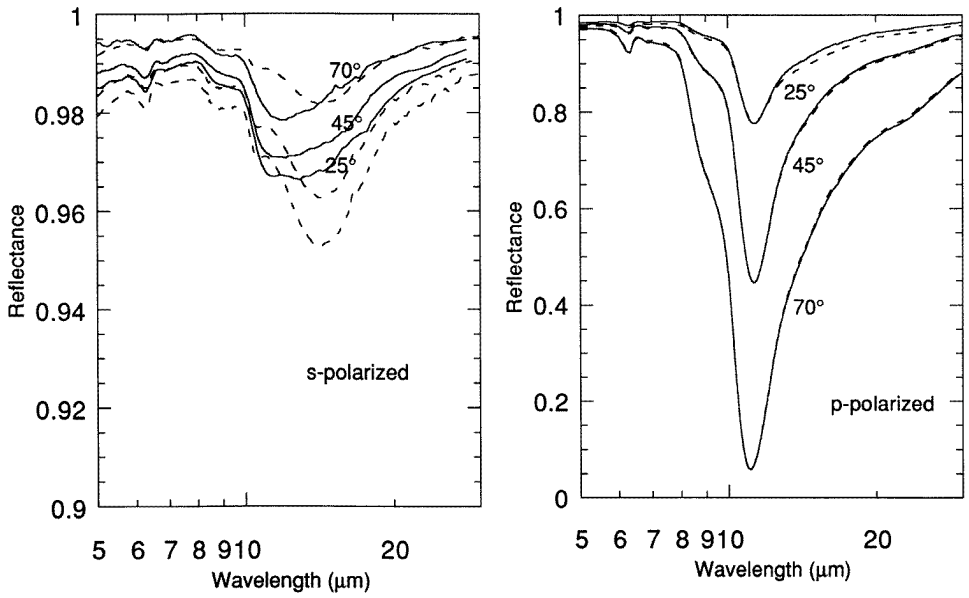

Figure 2. Specular reflectance for angles of incidence 25°, 45° and 70°, experimental and calculated using the experimentally derived refractive index. The experimental curves are drawn as solid lines.

(i) The real part of the dielectric function is reduced and the function has no zero for the porous alumina.

(ii) The maximum of the imaginary part for the porous oxide is about two thirds of the value for the non-porous oxide, but there is no shift of the peak located at 15.9 μm. The half-width–maximum ratio is similar for the two types of alumina. The second maximum at 26 μm is not clearly seen from the porous oxide data because of the large errors in this wavelength region. However, a linear fit to the data actually indicates that this second maxima is also present for the porous oxide.

(iii) The maximum of the dielectric loss function representing the LO mode is shifted from 10.6 μm for the non-porous oxide to 11.4 μm for the porous oxide. Again, the peak value of the porous oxide is about two thirds of that of the non-porous one and the peak is broader.

A model has been proposed in which the amorphous system has a Gaussian distribution of oscillators, each oscillator having a small Lorentzian damping [10]. This model has been used to fit reflectance data from thin alumina films on silicon, and the result was considerably better than that obtained using a classical Lorentz model. The same model can be applied to these data since the shape of ε'' in figure 3 for both porous and non-porous oxides is not Lorentzian, but, rather, is more Gaussian in form.

The main features of the dielectric function in the reststrahlen band depend on the phonon modes, their damping and the electronic contribution to the dielectric function. By definition [23] wavelengths of longitudinal and transverse optical phonon modes are determined from the zero and pole of the dielectric function $\varepsilon' = \varepsilon' + \mathrm{i}\varepsilon''$ for a system with no damping. For a heavily damped system, as in this case, there is neither a zero nor a pole for the dielectric function for real wavelengths [23]. The LO mode can be approximately

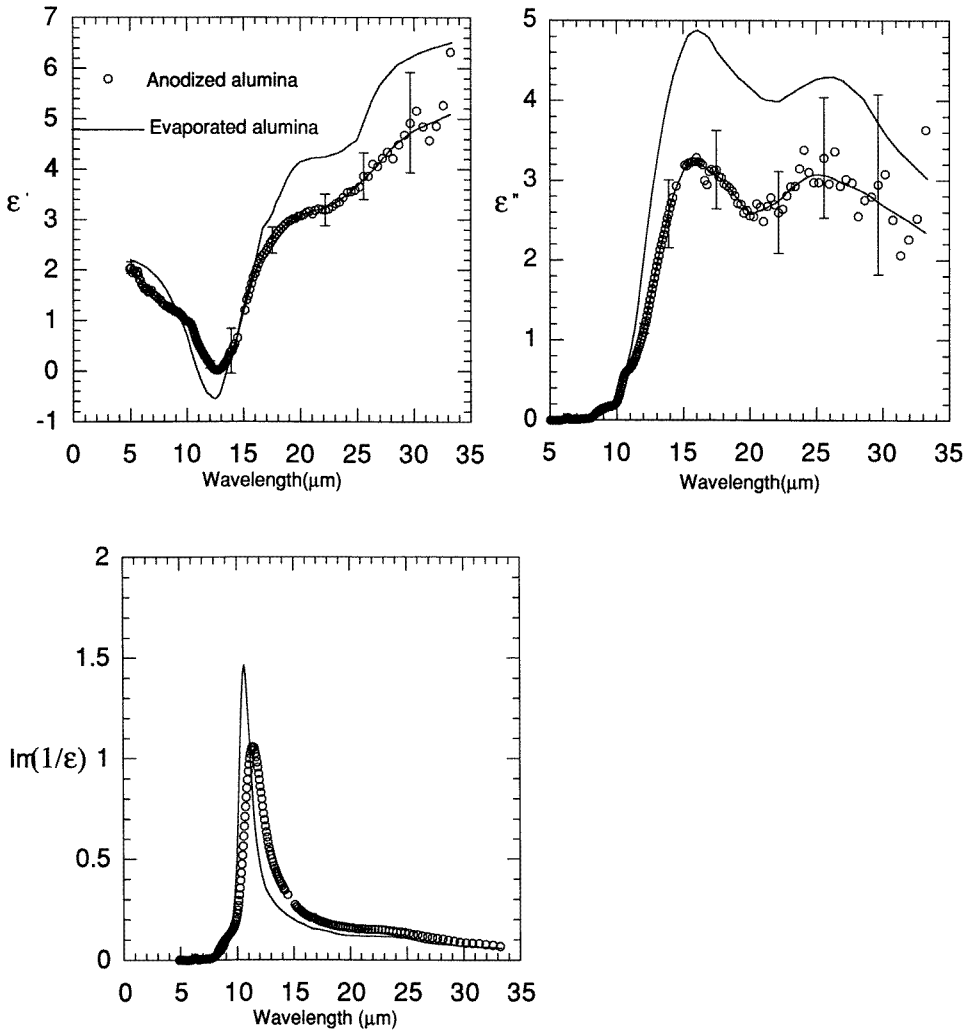

Figure 3. The dielectric function and energy-loss function of porous alumina. Line fits are drawn as a guide to the eye. For comparison the dielectric function of evaporated non-porous alumina [1] is presented in the figure.

defined as the minimum of $|\varepsilon|$ and the TO mode as the maximum of $|\varepsilon|$ [23], or as the maximum of $\mathrm{Im}(1/\varepsilon)$ and maximum of ε'', respectively [1].

According to Berreman's thin-film approximations [4] the p-polarized reflectance of a dielectric film on a metal substrate exhibits a minimum at the maximum of the energy-loss function, $\mathrm{Im}(1/\varepsilon)$, which means that for a slightly damped system the LO modes can be determined from this minimum of reflectance. For amorphous alumina the damping is so strong that the minimum of $|\varepsilon|$ is shifted to a shorter wavelength compared to the maximum of $\mathrm{Im}(1/\varepsilon)$, so the reflectance minimum should not be identified as the accurate wavelength of the LO phonon frequency. The shift of the minimum in the p-polarized reflectance for porous relative to non-porous alumina cannot be ascribed to a shift in the actual LO mode frequency only from such measurements. A shift in the LO mode frequency could be the

result of changes in the chemical bonds; thus a shift should also be expected for the TO mode frequency. According to the results above there is no wavelength shift for ε'' corresponding to a TO mode shift. Based on these results, it is expected that the chemical structure is similar for both porous and non-porous alumina. This is also confirmed by calculations of the radial distribution function (RDF) from x-ray diffraction data for amorphous alumina films prepared by evaporation (non-porous) [24], and anodization (porous) [25], with only small differences in nearest-neighbour distances and coordination numbers [26, 27]. The amorphous short-range order can be described as aluminium located predominantly in tetrahedral sites in a close-packed oxygen random network.

If a change in chemical bonding is not the main reason for the LO mode shift, the actual presence of the pores could be. Since the pores have dimensions much less than the wavelength, an effective medium can be used to describe the porous alumina when interacting with infrared light.

The Maxwell-Garnett and Bruggemann effective-medium models [28, 29, 30] for a two-component inhomogeneous material were used to calculate the dielectric function for air-filled pores. The basic definition of an effective medium is that a random unit cell, when embedded in the effective medium, should not be detectable in an experiment using electromagnetic radiation confined to a specific wavelength range. Effective-medium theory, EMT, is valid for inhomogeneous two-component materials when the size of at least one of the components is less than the wavelength of the light used in the measurement. This condition is fulfilled in this context since the pore dimension is less than the infrared wavelength. The Maxwell-Garnett model of the inhomogeneous medium is closest to the morphology of the anodic film, with well separated grains, the pores, embedded in a continuous host of alumina. Calculations were also executed with the Bruggemann model for comparison. This model is better suited for aggregate structures in which the two components appear in equal distributions to form a space-filling random mixture. The results appeared to be independent of the model in the wavelength range analysed, and for that reason only the calculations made using the Maxwell-Garnett effective dielectric function are presented here since it has an analytic form. The effective dielectric function is a function of the pore filling factor, the dielectric function of the constituents, and the shape of the pores—which determines the depolarization field of the pores and the surrounding alumina.

The Maxwell-Garnett effective dielectric function for elliptical particles can be expressed as [31]

$$\varepsilon = \varepsilon_{\text{alumina}} \frac{\varepsilon_{\text{alumina}}(1 - L_{x,z}^{\text{pore}} + L_{x,z}^{\text{pore}})\varepsilon_{\text{pore}} + f(1 - L_{x,z}^{\text{alumina}})(\varepsilon_{\text{pore}} - \varepsilon_{\text{alumina}})}{\varepsilon_{\text{alumina}}(1 - L_{x,z}^{\text{pore}}) + L_{x,z}^{\text{pore}}\varepsilon_{\text{pore}} - f L_{x,z}^{\text{alumina}}(\varepsilon_{\text{pore}} - \varepsilon_{\text{alumina}})}.$$

The symbol $L_{x,z}$ denotes the depolarization factor in the direction of the incoming electromagnetic radiation, the x-direction in the surface plane and the z-direction perpendicular to the surface. For simplicity, the depolarization factors are set equal for both pores and alumina, a condition which is valid for f close to unity, where f is the filling factor of the total pore volume relative to the total volume. The shapes of the pores are simplified to the geometry of long cylinders perpendicular to the surface. The dielectric function was calculated for the two directions of highest symmetry of the cylinder: ε_z, parallel, and ε_x, perpendicular to the long axis of the cylinder. The z-component here is parallel to the surface normal. The depolarization factors in these directions are 0 and 0.5 respectively. The dielectric function of the electron-beam-evaporated aluminium oxide [11] was used for alumina. The volume fraction of air-filled pores found from TEM, 0.3, was used. The equations for the effective dielectric function for the Maxwell-Garnett theory

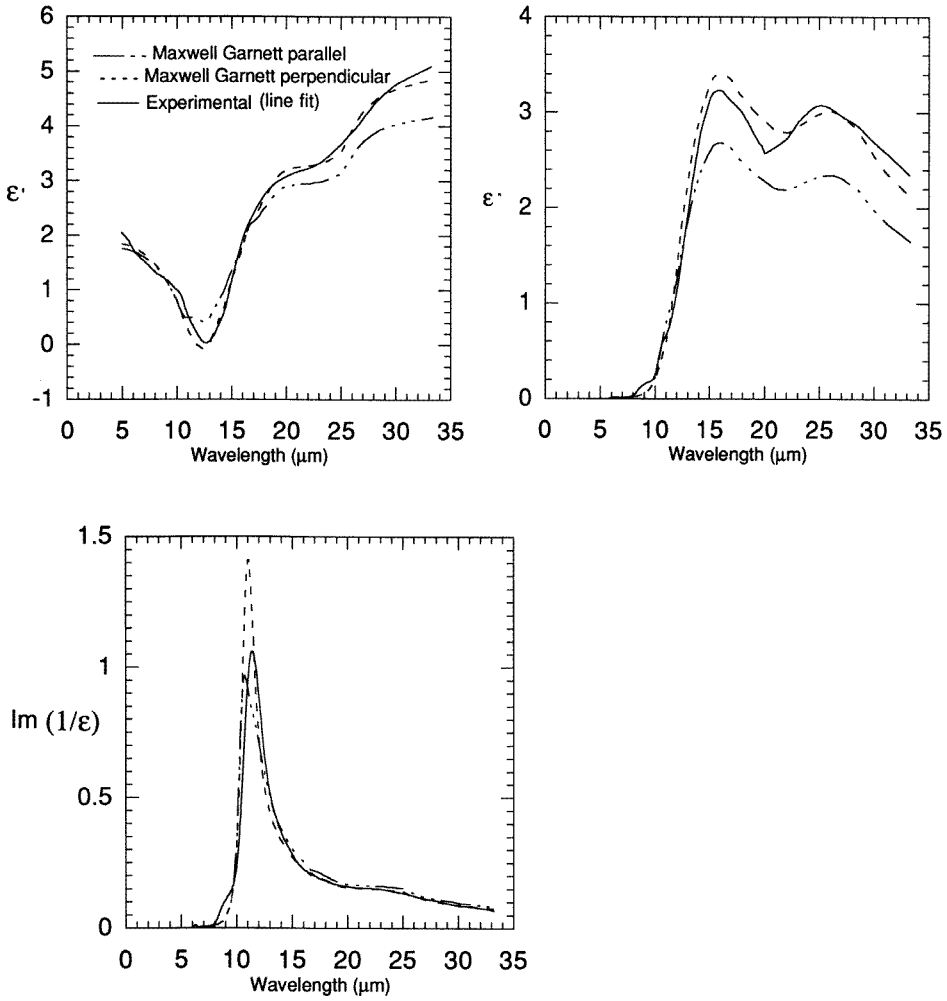

Figure 4. The effective dielectric function, obtained using Maxwell-Garnett effective-medium theory, is compared with the experimental dielectric function. The filling factor is 0.3 and the pores are regarded as cylinders perpendicular to the surface. The figure shows the components of the theoretical dielectric function and energy-loss function parallel and perpendicular to the surface.

with the appropriate numerical values for the depolarization and filling factors were

$$\varepsilon_z = 0.3\varepsilon_{\text{pore}} + 0.7\varepsilon_{\text{alumina}}$$

$$\varepsilon_x = \varepsilon_{\text{alumina}}(0.65\varepsilon_{\text{pore}} + 0.35\varepsilon_{\text{alumina}})/(0.35\varepsilon_{\text{pore}} + 0.65\varepsilon_{\text{alumina}}).$$

Figure 4 shows the experimental and calculated dielectric functions and demonstrates that there is good agreement, especially with ε_z, which was expected since high-angle p-polarized reflectance has been used to determine the dielectric function. For the energy-loss function, however, the computed peak for ε_z has shifted to longer wavelengths compared to the energy-loss function of the plain oxide, from 10.6 to 10.9 μm (i.e., 943 to 917 cm^{-1}). The theoretical peak is higher and narrower than the experimental one, but the integrated energy loss of the wavelength range of figure 4 is the same for both. To obtain the larger

experimental shift, the pore fraction must be as high as 0.45 which is not realistic according to the TEM measurements.

7. Conclusion

Substantial absorption of electromagnetic radiation occurs for wavelengths where the radiation couples with the longitudinal optical phonon. The absorption is nearly 100% for a 0.5 μm alumina film on an aluminium substrate for oblique incidence. The method of using reflectance measurements to determine optical constants is rather limited, but it can be used in the reststrahlen band wavelength range for thin amorphous alumina films using p-polarized light at two high angles of incidence. Anodic porous alumina is anisotropic since the pores are developed as channels perpendicular to the surface. The dielectric function derived from high-angle p-polarized reflectance should then be similar to the element in the dielectric tensor of an anisotropic medium which is perpendicular to the surface. The dielectric function perpendicular to the surface calculated from Maxwell-Garnett effective-medium theory and the experimental dielectric function are in good agreement. The peak in ε'' at 15.9 μm (630 cm^{-1}) is not shifted for an effective medium composed of air-filled pores in alumina from its position for non-porous alumina. This implies that the differences between porous and non-porous alumina originate mainly from the pores, not from differences in chemical bonds. This conclusion is also confirmed by the wavelength shift of the peak in the energy-loss function found both theoretically and experimentally for porous alumina compared to non-porous alumina, although the theoretical shift is smaller. The wavelength shift is also seen in the reflectance minima for p-polarized light at a non-normal angle of incidence.

Acknowledgments

Dr Gunnar Niklasson is acknowledged for good advice and fruitful discussions, research engineer Rein Kalm for assisting with SEM and TEM measurements and Fil. Lic. Nils-Olov Ersson for the x-ray diffraction analyses. This work was financed by the Swedish Council for Building Research (BFR) and the Marcus and Amalia Wallenberg Foundation.

References

[1] Barker A S 1963 *Phys. Rev.* **132** 1474–81
[2] Chu Y T, Bates J B, White C W and Farlow G C 1988 *J. Appl. Phys.* **64** 3727–30
[3] Yamamoto J 1979 *Cryogenics* **19** 87–8
[4] Berreman D W 1963 *Phys. Rev.* **130** 2193–8
[5] Brüesch P, Kötz R, Neff H and Pietronero L 1984 *Phys. Rev.* B **29** 4691–6
[6] Chatelet J, Claassen H H, Gruen D M, Sheft I and Wright R B 1975 *Appl. Spectrosc.* **29** 185–9
[7] Handke M, Paluszkiewicz C and Wyrwa W 1981 *Mater. Chem.* **6** 197–208
[8] Maeland A J, Rittenhouse R, Lahar W and Romano P V 1974 *Thin Solid Films* **21** 67–72
[9] Takamura T, Kihara-Morishita H and Moriyama U 1970 *Thin Solid Films* **6** R17–R19
[10] Brendel R and Bormann D 1992 *J. Appl. Phys.* **71** 1–6
[11] Eriksson T S, Hjortsberg A, Niklasson G A and Granqvist C G 1981 *Appl. Opt.* **20** 2742–6
[12] Harris L 1955 *J. Opt. Soc. Am.* **45** 27–9
[13] Harris L and Piper J 1962 *J. Opt. Soc. Am.* **52** 223–4
[14] Pavlovic T and Ignatiev A 1986 *Thin Solid Films* **138** 97–109
[15] Keller F, Hunter M S and Robinson D L 1953 *J. Electrochem. Soc.* **100** 411–9
[16] Nakamura S, Saito M, Huang L F, Miyagi M and Wada K 1992 *Japan. J. Appl. Phys.* **31** 3589–93
[17] Blain J, LeBel C, Saint-Jacques R G and Rheault F 1985 *J. Appl. Phys.* **58** 490–4

[18] Tanemura S, Yoshimura K, Taga K, Odaira R, Ishida M, Tsuboi M and Yoshikawa M 1990 *Int. Solar Energy Society Congress (1989)* (Kobe, Japan: Pergamon) pp 2267–71
[19] Shiles E, Sasaki T, Inokuti M and Smith D Y 1980 *Phys. Rev.* B **22** 1612
[20] Lan T T, Naudin F and Robbe-Bourget P 1964 *J. Physique* **25** 11–4
[21] Ward L 1988 *The Optical Constants of Bulk Materials and Films (The Adam Hilger Series on Optics and Optoelectronics)* ed E R Pike and W T Welford (Bristol: Hilger)
[22] Smith G B 1990 *Appl. Opt.* **29** 3685–93
[23] Chang I F, Mitra S S, Plendl J N and Mansur L C 1968 *Phys. Status Solidi* **28** 663–73
[24] Manaila R, Dévényi A and Candet E 1984 *Thin Solid Films* **116** 289–99
[25] Chernykh M A, Belov V T, Terekhov V A and Amirova N A 1988 *Izv. Akad. Nauk SSSR, Neorg. Mater.* **24** 1127–31
[26] Oka Y and Takahashi T 1979 *J. Non-Cryst. Solids* **30** 349–57
[27] Despić A and Parkhutik V P 1989 *Electrochemistry of Aluminum in Aqueous Solutions and Physics of Its Anodic Oxide (Modern Aspects of Electrochemistry)* ed J O Bockris, R E White and B E Conway (New York: Plenum)
[28] Garnett J C M 1904 *Phil. Trans. R. Soc.* **203** 385–420
[29] Garnett J C M 1906 *Phil. Trans. R. Soc.* **205** 237–88
[30] Bruggeman D A G 1935 *Ann. Phys., Lpz.* **24** 636–78
[31] Bilboul R R 1969 *J. Phys. D: Appl. Phys.* **2** 921–3